




# Design and Validation of a Multi-objective Automotive State Estimator for Unobservable and Non-linear Vehicle Models

Thijs Devos<sup>1,2</sup><sup>a</sup>, Matteo Kirchner<sup>1,2</sup><sup>b</sup>, Jan Croes<sup>1,2</sup><sup>c</sup>, Jasper De Smet<sup>3</sup><sup>d</sup> and Frank Naets<sup>1,2</sup><sup>e</sup>

<sup>1</sup>*LMSD Research Group, Department of Mechanical Engineering, KU Leuven, Celestijnenlaan 300, 3001 Leuven, Belgium*

<sup>2</sup>*DMMS Core Lab, Flanders Make, Gaston Geenslaan 8, 3001 Leuven, Belgium*

<sup>3</sup>*MotionS Core Lab, Flanders Make, Gaston Geenslaan 8, 3001 Leuven, Belgium*

**Keywords:** State Estimation, Extended Kalman Filter, Observability, Sensor Selection, Non-linear Vehicle Model.


**Abstract:** This paper presents a novel automotive state estimation approach aiming to provide reliable results for multi-objective estimation applications. Because single-objective estimators typically feature simple, dedicated models, they often lack accuracy for highly dynamically coupled systems such as vehicles. Therefore, this approach features a more complex, system-level, non-linear vehicle model containing more accurate physics. Based on the assumption that the estimator targets a specific number of quantities of interest, an extensive observability analysis is performed to ensure stable estimator operation. Firstly, a novel algorithm to detect unobservable estimator states is presented, followed by a methodology for detailed analysis on which estimator states are decoupled using the linearized Jacobians. It is shown that if the unobservable states are partially decoupled and have no dependency towards the quantities of interest, an observable transformation can be carried out which stabilizes the estimator during the operation ensuring reliable and interpretable results for the quantities of interest. The methodology is validated using an experimental vehicle case for which sensor selection was performed and demonstrates the estimator performance as well as potential limitations for unobservable vehicle states.


## 1 INTRODUCTION


Nowadays, vehicles are becoming more complex with many integrated subsystems, designed to meet stricter requirements towards safety, comfort and emissions. This increase of complexity has led to the development of Advanced Driver Assistance Systems (ADAS) which require accurate knowledge on vehicle states, inputs and parameters to work adequately. However, direct measurement of these variables is often impossible, or the required sensors are costly or impractical to implement (e.g. tire force transducers, optical sensors,...). As a result of this, the development of advanced estimation algorithms has gained significant traction in the past years as it provides a cost-effective solution to this problem.


Currently, automotive estimators are typically de-


signed for obtaining accurate information on one specific quantity of interest such as the sideslip angle, tire forces or the friction coefficient (e.g. in (Albinsson et al., 2014), (Wang and Wang, 2013)). The main benefit of this approach is that the exploited models can be kept relatively simple, dedicated and tailored to the application which requires less implementation and computational effort. However, with the rising complexity of commercial vehicles, these simple, dedicated models fail to sufficiently capture the physics involved leading to impaired estimation results for highly dynamically coupled systems such as vehicles. Additionally, many control algorithms require a multitude of hardly measurable quantities at the same time such that multi-objective estimators deserve special attention. These multi-objective estimators also require that the necessary physics are sufficiently captured by the model. This leads to the need for more complex, non-linear vehicle models in estimation algorithms. Solutions dealing with non-linear vehicle models were already presented, for example in (Reif et al., 2007), (Nakamura et al., 2020) and have been

<sup>a</sup>  <https://orcid.org/0000-0001-9130-9449>

<sup>b</sup>  <https://orcid.org/0000-0002-3060-8100>

<sup>c</sup>  <https://orcid.org/0000-0003-3339-5718>

<sup>d</sup>  <https://orcid.org/0000-0002-7885-1839>

<sup>e</sup>  <https://orcid.org/0000-0002-5228-7395>

proven to work sufficiently well for very simple vehicle models but not yet for larger, more complex models. Furthermore, vehicle estimators exploiting more complex models often experience difficulties dealing with unobservable position states when GPS measurements are unavailable, either because the sensor is unavailable or has lost communication to the satellites. On top of that, GPS measurements are often irrelevant for the estimation of common quantities of interest targeted by automotive estimators. Solutions have been proposed in literature to overcome observability issues, varying from not including the position states to the governing equations (Kim et al., 2020) to simply omitting the contributions of unwanted states from the covariance equations (Yang et al., 2010). However, since most of these estimators feature dedicated models, also the solutions to overcome observability are tailored to the application and thus not always applicable. In general, a better approach to develop an automotive estimator would be to immediately design the estimator to target multiple quantities of interest exploiting a system-level, non-linear model with special attention towards analysing observability.

This paper therefore starts from a multi-objective automotive estimator methodology featuring a system-level, non-linear vehicle model. Due to the multi-objective nature of the estimator, additional analysis towards observability and sensor selection are addressed in this work. It is shown that, due to the partially decoupled nature of vehicle position states, GPS measurements are crucial to obtain observable trajectory states but do not contribute to the estimation of for example tire forces. Using an observable projection, the unobservable and decoupled state covariances can be stabilized. Next to this, sensor selection was performed by ranking the sensors according to their contributions to the estimation performance expressed by the quantity of interest covariance. Finally, the proposed estimator has been validated on an experimental vehicle case for a low excitation maneuver which demonstrates its potential and shows potential limitations for unobservable states.

## 2 AUTOMOTIVE STATE ESTIMATION USING A NON-LINEAR VEHICLE MODEL

Figure 1 shows a schematic overview of the proposed estimator approach. The estimator exploits an Extended Kalman Filter (EKF) using a system-level,

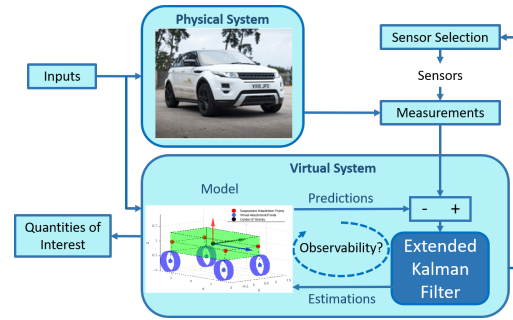


Figure 1: Schematic overview of the estimator presented in this work.

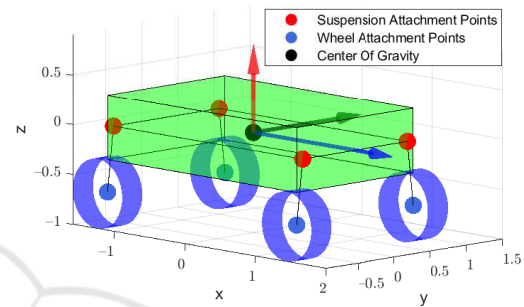


Figure 2: The system-level, non-linear 10 DOF vehicle model used in the estimator.

non-linear vehicle model which is depicted on Figure 2. The estimator methodology is based on the work of (Devos et al., 2021) and uses three non-linear equations for the model, measurements and quantities of interest:

$$\text{Model: } \dot{\mathbf{x}} = \mathbf{f}(\mathbf{x}, t) \quad (1)$$

$$\text{Measurements: } \mathbf{y} = \mathbf{h}(\mathbf{x}, t) \quad (2)$$

$$\text{Quantities of Interest: } \mathbf{y}_{vs} = \mathbf{g}(\mathbf{x}, t) \quad (3)$$

where the (non-linear) functions  $\mathbf{f}$ ,  $\mathbf{h}$  and  $\mathbf{g}$  represent respectively the model, measurement and quantities of interest equations. The state vector is represented by  $\mathbf{x}$  and  $t$  is the time.

### 2.1 Vehicle Model

Starting from the model as developed by (Vaseur et al., 2020), the suspension characteristic curves were tuned and the tire model was adjusted to increase accuracy for low velocities. The complete vehicle model consists of 16 states corresponding to 10 Degrees Of Freedom (DOFs) of which 6 are represented by the vehicle chassis (3 translational and 3 rotational) and 4 are related to the wheel rotations. While the general equations of motion for the vehicle chassis and the wheels can be found in (Vaseur et al., 2020), the following subsections present the suspension model and tire model used for this application as they were optimized for this particular estimator case.

### 2.1.1 Suspension Model

From experimental data presented in section 4, it has been proven that the stiffness curve of the suspension can be approached better using a non-linear relation. This allows the model to represent the physical system better and will therefore further enhance estimation performance. Additionally, less tuning of the estimator noise matrices is required to acquire accurate results. The stiffness curve can be expressed as a function of the form:

$$F_{z,k} = Ae^{(B|r_{sa}-r_{wa}|)} \quad (4)$$

where  $|r_{sa} - r_{wa}|$  is the distance from the suspension attachment point to the wheel attachment point and  $A$  and  $B$  are parameters defined to tune the curve. The stiffness curve parameters were determined by fitting the non-linear curve through experimental data using a non-linear least squares method. The parameters were set to  $A = 500$  and  $B = 14$  which leads to the fitted data presented in the upper graph of figure 3.

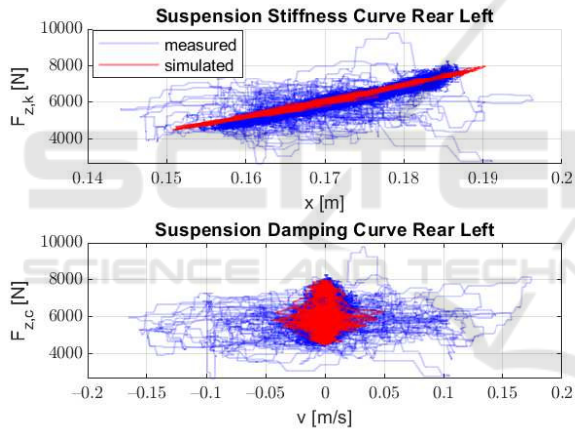


Figure 3: The non-linear suspension stiffness (upper) and linear suspension damping (lower) curve.

Next to this, a linear damping model is used with the following characteristic equation:

$$F_{z,c} = cv \quad (5)$$

where  $c$  is the damping constant and  $v$  the velocity of the suspension attachment point in the direction of the suspension strut. Similar to the stiffness parameters, the damping constant has also been tuned based on experimental data and has been set to 5000Ns/m. The lower graph of figure 3 compares the simulated versus the measured damping curve for this parameter. The overall suspension force is then calculated by summing the contributions from the stiffness and damping curve:

$$F_z = F_{z,k} + F_{z,c} \quad (6)$$

### 2.1.2 Tire Model

The tire model used in this paper is a linear tire model using constant cornering stiffnesses. This choice was made because for the tests discussed in this paper, the vehicle did not enter the non-linear part of the tire characteristic and therefore the extension towards a non-linear tire model is not needed.

The calculation of the tire forces starts with the derivation of the longitudinal slip and sideslip angle for each tire. In this work, the formulas are based on the brush model (Svendenius and Wittenmark, 2003) but altered slightly to prevent singularities at low velocities or wheel lock-up:

$$\kappa_{ij} = \begin{cases} \frac{v_{x,ij} - \omega_{ij}r_{whl}}{|v_{x,ij}|} & \text{if } v_{x,ij} \geq 1 \\ v_{x,ij} - \omega_{ij}r_{whl} & \text{if } v_{x,ij} < 1 \end{cases} \quad (7)$$

$$\alpha_{y,ij} = \begin{cases} \frac{v_{y,ij}}{|v_{x,ij}|} & \text{if } v_{x,ij} \geq 1 \\ v_{y,ij} & \text{if } v_{x,ij} < 1 \end{cases} \quad (8)$$

where  $v_{x,ij}$  is the longitudinal wheel velocity. Here, the index  $i$  indicates front or rear and  $j$  indicates left or right. Furthermore,  $v_{y,ij}$  represents the lateral wheel velocity,  $\omega_{ij}$  the wheel angular velocity and  $r_{whl}$  is the wheel radius.

Furthermore, the tire forces can be expressed using a linear tire model with constant cornering stiffnesses by the following equations for respectively the longitudinal and lateral force:

$$F_{x,ij} = C_{x,i}\kappa_{ij} \quad (9)$$

$$F_{y,ij} = C_{y,i}\alpha_{y,ij} \quad (10)$$

where the cornering stiffnesses  $C_{x,i}$  and  $C_{y,i}$  were obtained experimentally using tire force transducers. In these equations,  $\kappa_{ij}$  represents the longitudinal slip and  $\alpha_{y,ij}$  the sideslip angle of each wheel.

## 2.2 Measurement Equations

In this work, sensors are considered which are commonly mounted on commercial vehicles or sensors which could potentially significantly improve estimation performance. These sensors include body accelerations, yaw rate, suspension stroke measurements, longitudinal and lateral velocity, wheel speed encoders and the GPS. The measurement vector for these respective sensors can be expressed as:

$$y = [\dot{v}_{cog} \quad \omega_z \quad |r_{sus}| \quad v_x \quad v_y \quad \dot{\omega}_{ij} \quad x \quad y]^T \quad (11)$$

where  $|r_{sus}| = |r_{sa,ij} - r_{wa,ij}|$  and  $r_{sa,ij}$  is the location of the suspension attachment point and  $r_{wa,ij}$  is the location of the wheel attachment point. All other measurements are states of the estimator.

### 2.3 Quantities of Interest

The quantities of interest need to be defined which will be the targets of the estimator. Since this paper presents an approach for multi-objective estimation, multiple quantities of interest are defined. Therefore, the following quantities of interest are targeted by the estimator:

- Rear left wheel forces ( $F_{x,rl}$ ,  $F_{y,rl}$  and  $F_{z,rl}$ )
- Sideslip angle at body center of gravity ( $\beta$ )
- Vehicle trajectory ( $x, y$ )

The complete quantities of interest vector can thus be expressed as:

$$\mathbf{y}_{vs} = [F_{x,rl} \ F_{y,rl} \ F_{z,rl} \ \beta \ x \ y] \quad (12)$$

$$= [F_{x,rl} \ F_{y,rl} \ F_{z,rl} \ \arctan\left(\frac{y}{x}\right) \ x \ y] \quad (13)$$

where the tire forces  $F_{x,rl}$ ,  $F_{y,rl}$  and  $F_{z,rl}$  are calculated as mentioned in (Vasseur et al., 2020) and  $x$  and  $y$  are the position states of the estimator.

Tire forces and the sideslip angle are selected as these variables are useful for advanced control algorithms but not directly measurable in a cost-effective manner. Additionally, the vehicle position is chosen to showcase the benefits of the observability analysis presented in section 3 on a real vehicle case as these states are commonly unobservable in automotive estimators.

### 2.4 Extended Kalman Filter Application

In this work, the Extended Kalman Filter (EKF) is selected as this filter is a straightforward extension of the efficient linear Kalman filter for non-linear systems. Linearization, discretization and estimator set up are performed according to the work in (Devos et al., 2021). For this particular application, the discretized dynamic state-space equations form the basics of the estimation framework and can be expressed using the linearized Jacobians as:

$$\mathbf{x}_{k+1} = \mathbf{F}_k \mathbf{x}_k + \mathbf{B}_k \mathbf{u}_k \quad (14)$$

$$\mathbf{y}_{k+1} = \mathbf{H}_k \mathbf{x}_{k+1} \quad (15)$$

$$\mathbf{y}_{vs,k+1} = \mathbf{G}_k \mathbf{x}_{k+1} \quad (16)$$

where  $\mathbf{F}$  is the system Jacobian matrix,  $\mathbf{x}$  is the state vector,  $\mathbf{y}$  is the measurement vector,  $\mathbf{H}$  is the measurement Jacobian,  $k$  is the timestep and  $\mathbf{B}$  and  $\mathbf{u}$  are respectively the input Jacobian and the input vector. Here, the linearized Jacobians  $\mathbf{F}_k$ ,  $\mathbf{H}_k$  and  $\mathbf{G}_k$  are saved every timestep for use during the observability analysis as discussed in section 3. Finally, they are used to calculate the EKF covariance equations and state updates as documented in (Devos et al., 2021).

### 2.5 Sensor Selection

As a final point of attention, this work aims at selecting the appropriate sensors for the estimation application using the methodology presented in (Devos et al., 2021). The methodology proposes to evaluate the sensor performance before they are acquired based on their relative contribution to the quantities of interest covariance and has proven to deliver consistent results for non-linear models.

## 3 OBSERVABILITY ANALYSIS

Observability is an important estimator property which determines whether the targeted quantities of interest can be estimated with a bounded uncertainty. As this work features an EKF based framework, the Jacobians are linearized every timestep and therefore the result of linear observability tests can also change. To analyze global observability, the total observability matrix is used which combines observability matrices calculated at evenly spaced timesteps and can be expressed as:

$$O_{tot} = \begin{bmatrix} O_1 \\ O_{1+p} \\ O_{1+2p} \\ \vdots \\ O_m \end{bmatrix} \quad (17)$$

where the integer parameter  $p$  indicates how many observability matrices are taken into account.

### 3.1 Determining Unobservable States

Using the previously defined total observability matrix, information can be extracted on which states are unobservable. The first step is to calculate the kernel of the total observability matrix:

$$\mathbf{V}_u = \text{null}(O_{tot}) \quad (18)$$

The resulting matrix  $\mathbf{V}_u$  contains the vectors which span the null space of the observability matrix. If the total observability matrix is full of rank,  $\mathbf{V}_u$  will not contain any base vectors. However, if at least one state is unobservable,  $\mathbf{V}_u$  will contain as many vectors as unobservable states. Because the vectors of  $\mathbf{V}_u$  provide an orthogonal base to span the kernel of the observability matrix, the entire matrix  $\mathbf{V}_u$  will have near zero contributions except for the unobservable states which makes it possible to identify them. One possible algorithm is to check for non-zero contributions in the rows of the kernel vectors as described by algorithm 1. Here,  $n$  is the number of states and  $\mathbf{x}_u$  are

Algorithm 1: Unobservable state detection algorithm.

```

1:  $\mathbf{x}_u = []$ ;
2: for  $i = 1 : n$  do
3:   if  $\text{mean}(V_u(i,:)) > \text{threshold}$  then
4:      $\mathbf{x}_u = [\mathbf{x}_u, i]$ ;
    
```

the unobservable states as detected by the algorithm. The threshold value depends on the precision of the machine and was set to  $10^{-10}$  for this work. For the pseudo-code presented in algorithm 1, the assumption has been made that the columns of the matrix  $\mathbf{V}_u$  contain the kernel base vectors.

### 3.2 Dynamic Coupling Analysis using the Linearized System Jacobian

When the unobservable states have been identified, further analysis can be done on what causes these states to be unobservable. As the observability matrix is determined by the linearized system and measurement Jacobians  $\mathbf{F}_k$  and  $\mathbf{H}_k$ , unobservable states are the cause of both the lack of contributions in the measurement Jacobian and the lack of dynamic coupling between the vehicle states in the system Jacobian. This dynamic coupling heavily determines which measurements are needed to ensure full observability.

When the unobservable states have been determined, equations 14, 15 and 16 can be partitioned such that the unobservable states are gathered in the lower part of the state-space vector. The following model equation is obtained:

$$\begin{bmatrix} \dot{\mathbf{x}}_o \\ \dot{\mathbf{x}}_u \end{bmatrix}_{k+1} = \begin{bmatrix} \mathbf{F}_{oo} & \mathbf{F}_{ou} \\ \mathbf{F}_{uo} & \mathbf{F}_{uu} \end{bmatrix}_k \begin{bmatrix} \mathbf{x}_o \\ \mathbf{x}_u \end{bmatrix}_k + \begin{bmatrix} \mathbf{B}_o \\ \mathbf{B}_u \end{bmatrix}_k \mathbf{u}_k \quad (19)$$

where  $\mathbf{x}_o$  are the observable states and  $\mathbf{x}_u$  are the unobservable states. From this equation, the following cases can be derived:

**$\mathbf{F}_{ou} \neq \mathbf{0}$  &  $\mathbf{F}_{uo} \neq \mathbf{0}$ :** In this case, the model is highly coupled and the system Jacobian is fully occupied as depicted on the left matrix of figure 4. Here, sensors which have contributions to only a few states instantly cause all states to be theoretically observable due to the dynamic coupling in the model. In practice however, the coupling might be weak which can still lead to unobservable states.

**$\mathbf{F}_{ou} = \mathbf{0}$ :** In this case, the equations are partially decoupled and the system Jacobian is of the form as presented by the middle matrix of figure 4. A typical example are systems containing friction models as the friction force usually depends on the normal force but not vice versa.

**$\mathbf{F}_{ou} = \mathbf{0}$  &  $\mathbf{F}_{uo} = \mathbf{0}$ :** In this case, the equations are decoupled and the system Jacobian is of the form as presented by the right matrix of figure 4. For this case, no dynamic coupling exists between the states  $\mathbf{x}_o$  and  $\mathbf{x}_u$  in the model.

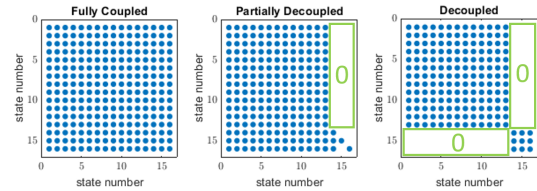


Figure 4: Different possible layouts of the system Jacobian matrix  $\mathbf{F}_k$ .

In this work, the vehicle model can be categorized by the second case where  $\mathbf{F}_{ou} = \mathbf{0}$ . The partially decoupled state vector  $\mathbf{x}_u$  consists of the vehicle longitudinal and lateral position. Because these states are partially decoupled, they will be unobservable if their corresponding measurements are not taken into account due to the lack of dynamic coupling. This leads to stability issues as the covariances of these states will be unbounded. In case these unobservable states do not depend on the quantities of interest, an observable transformation can be deployed to stabilize the unobservable covariances. The transformation can be expressed as:

$$\mathbf{x} = \mathbf{V}_o^T \mathbf{q} \quad (20)$$

where  $\mathbf{V}_o$  is the observable part of the mode matrix  $\mathbf{V}$  resulting from a Singular Value Decomposition (SVD) of the total observability matrix  $O_{tot}$ .

A final point of attention is that, even though the system Jacobian could be fully coupled, it might still occur that the observability matrix is ill-conditioned if the values inside the Jacobian matrix are very small. A weak coupling is then present between the states which means that they theoretically depend on each other, but in practice the coupling is so small that they can be unobservable.

## 4 EXPERIMENTAL RESULTS

The proposed estimator approach has been validated on an electric vehicle case namely the Range Rover Evoque shown on Figure 5. The data was generated during a test campaign at Ford Lommel Proving Ground by (Van Aalst et al., 2018) and (Vaseur et al., 2020) and graciously provided to us for validation of this work. The vehicle was equipped with an SBG Inertial Measurement Unit (IMU) to measure accelerations, velocities, positions and angles, a Corrsys Datron optical sensor to obtain the sideslip angle, sus-

pension stroke measurements and Kistler tire force transducers. The vehicle CAN bus was also logged to measure the inputs to the model namely the steering wheel angle, motor torques and brake torques. All relevant vehicle parameters used to evaluate the equations are defined in table 1.



Figure 5: The Range Rover Evoque used on test track 7 at Ford Lommel Proving Ground (Van Aalst et al., 2018).

Table 1: Vehicle model parameters for the Range Rover Evoque (Naets et al., 2017).

Vehicle Property	Abbr	Value
Vehicle mass	$m$	2408 kg
Roll moment of inertia	$I_x$	615 kgm <sup>2</sup>
Pitch moment of inertia	$I_y$	1546 kgm <sup>2</sup>
Yaw moment of inertia	$I_z$	3231 kgm <sup>2</sup>
Distance COG - front axle	$l_f$	1.439 m
Distance COG - rear axle	$l_r$	1.236 m
Track width front	$t_f$	1.625 m
Track width rear	$t_r$	1.625 m
Height of COG	$h_{COG}$	0.65 m
Front cornering stiffness	$C_{yf}$	88.500 N/rad
Rear cornering stiffness	$C_{yr}$	118.200 N/rad
Wheel radius	$r_{whl}$	0.3597 m
Wheel inertia	$I_{whl}$	4 kgm <sup>2</sup>

## 4.1 Covariance Tuning

In this work, the estimator has been tuned by trial-and-error. The following (constant) values were used to populate the noise matrix  $Q_d$ :

$$Q_{v_x, v_y, v_z} = 1 \cdot 10^{-4}, Q_{\dot{\phi}, \dot{\theta}, \dot{\psi}} = 1 \cdot 10^{-3}$$

$$Q_{x, y, z} = 1 \cdot 10^{-5}, Q_{\phi, \theta, \psi} = 1 \cdot 10^{-1}, Q_{\omega_{ij}} = 1 \cdot 10^{-5}$$

where  $Q_{v_x, v_y, v_z}$  represents the translational velocity noise,  $Q_{\dot{\phi}, \dot{\theta}, \dot{\psi}}$  the rotational velocities noise,  $Q_{x, y, z}$  the position noise,  $Q_{\phi, \theta, \psi}$  the angular noise and  $Q_{\omega_{ij}}$  the wheel angular velocity noise.

Subsequently, the measurement noise was derived from specification sheets and tests executed in previous work by (Van Aalst et al., 2018) and were defined as:

$$R_{a_i} = 3.1 \cdot 10^{-3} (m/s^2)^2, R_{gyr} = 2.5 \cdot 10^{-1} (m/s)^2$$

$$R_{GPS} = 2m^2, R_{\omega_{ij}} = 2.1 \cdot 10^{-1} (m/s)^2$$

where  $R_{a_i}$  is the MEMS accelerometer noise of the IMU,  $R_{gyr}$  the gyroscope noise of the IMU,  $R_{GPS}$  the GPS noise,  $R_{\omega_{ij}}$  the wheel speed encoder noise.

## 4.2 Results and Discussion

The results of this work are clustered in three main sections as elaborated upon in this paper. To start, the appropriate sensors were selected according to the methodology presented in subsection 2.5. Subsequently, the synchronization capabilities are shown together with the limitations for unobservable, decoupled states as discussed in section 3. Finally, the estimator multi-objective performance is discussed showing the results for the targeted quantities of interest.

### 4.2.1 Sensor Selection

Figure 6 shows the results of the sensor selection algorithm where the blue line indicates the rise in covariance when the sensor is removed from the estimator. The bar colors indicate whether observability is fulfilled (green), partially fulfilled but can be stabilized by the projection defined in section 3.2 (yellow) or not fulfilled (red).

The figure confirms that some sensors indeed have significant contributions to multiple quantities of interest. Accelerations for example are important when estimating tire forces as they are directly related to the forces in the equations of motion. Additionally, figure 6 also shows that for the planar tire forces ( $F_x$  and  $F_y$ ), the yaw rate ( $\dot{\psi}$ ) is an important sensor whereas for the vertical tire force, the suspension stroke measurements are more important. On the other hand, GPS measurements are less relevant for the tire forces but are required when the vehicle trajectory states are part of the targeted quantities of interest. As indicated by the yellow and red bar colors, position states are automatically unobservable when GPS measurements are omitted due to their decoupled nature. All of the conclusions based on the results presented in figure 6 stroke with engineering experiences.

To ensure a good tracking of all the quantities of interest as defined in subsection 2.3, the results presented in figure 6 together with availability on commercial vehicles and cost were used to select the sensors for this estimator. In the end, the following sensors were chosen:

- Body accelerations ( $a_x$ ,  $a_y$  and  $a_z$ )
- Yaw rate ( $\dot{\psi}$ )
- Wheel speed encoders ( $\omega_{ij}$ )
- GPS ( $x$ ,  $y$ )

### 4.2.2 Synchronization Capabilities and Observability Analysis

When the vehicle trajectory states are part of the estimator quantities of interest, GPS measurements are

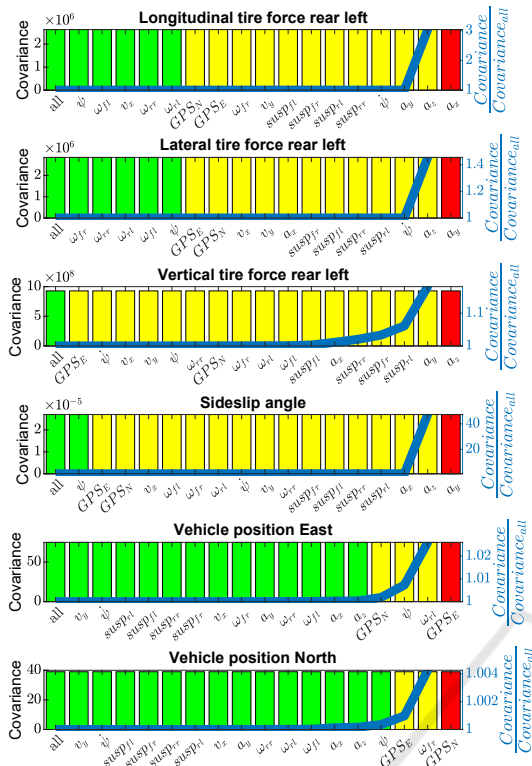


Figure 6: Results of the sensor selection ranking procedure. The x-axis represents cumulative removed sensors from the sensor space. The color of the bars indicate observability (green is observable, yellow is unobservable but stable and red is unobservable and unstable). The blue line visualizes the normalized covariance rise when omitting sensors.

important to deliver interpretable results. This is because these states are partially decoupled from the other ones as discussed in section 3 and therefore require GPS measurements to be observable. Figure 6 confirms this because, for every quantity of interest, as soon as the GPS measurement in either  $x$  or  $y$  direction is omitted, the yellow bar indicates that the estimator is unobservable but can be stabilized using the transformation defined in equation 20. Figure 7 shows that for unobservable position states, the vehicle trajectory is not correctly tracked even when applying the observable transformation of equation 20 which stabilizes the position covariances. Therefore, unobservable states and their associated covariances cannot be reliably interpreted and should be handled with care.

Figure 8 compares the simulated vehicle velocities and yaw rate versus measurements. These variables show that the estimator can synchronize the model well with the measurements using previously selected sensors. Additionally, these variables are currently widely used in ESP systems of commercial vehicles

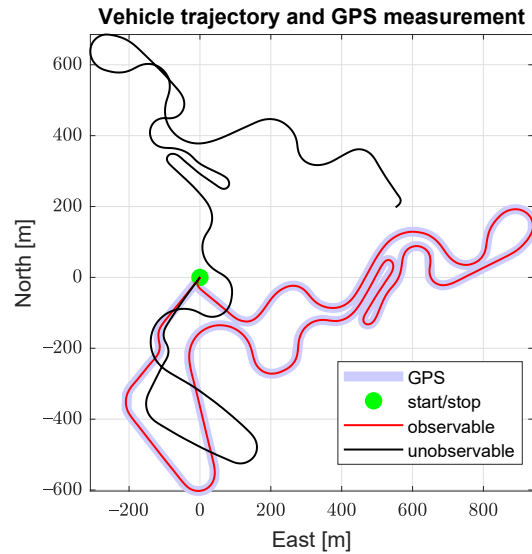


Figure 7: Simulated versus GPS measured trajectory for both an unobservable and observable simulation.

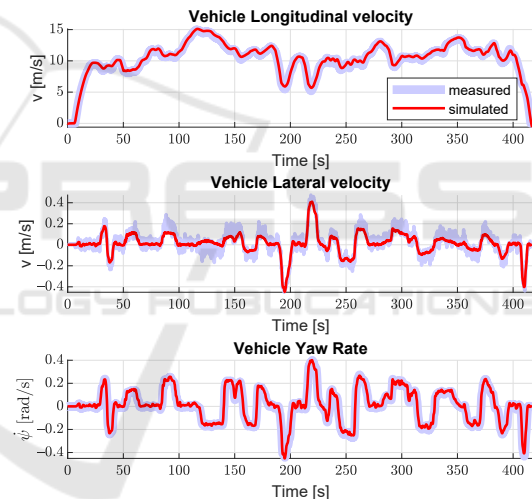


Figure 8: Estimation results versus measurements for the validation case: planar velocities and yaw rate.

and could therefore also be targeted by the estimator for use in advanced control algorithms.

### 4.2.3 Multi-objective Estimation

The resulting tire forces and vehicle sideslip angle can be seen in figure 9. The figure shows that the estimator is capable of determining the tire forces as well as the vehicle sideslip angle although the lateral tire forces are slightly over-estimated compared to the measurements. A possible explanation is that the road is assumed flat as including road angles is not a straightforward task. Nevertheless, the estimator shows reliable results for the targeted quantities of interest. When comparing to similar results for single-

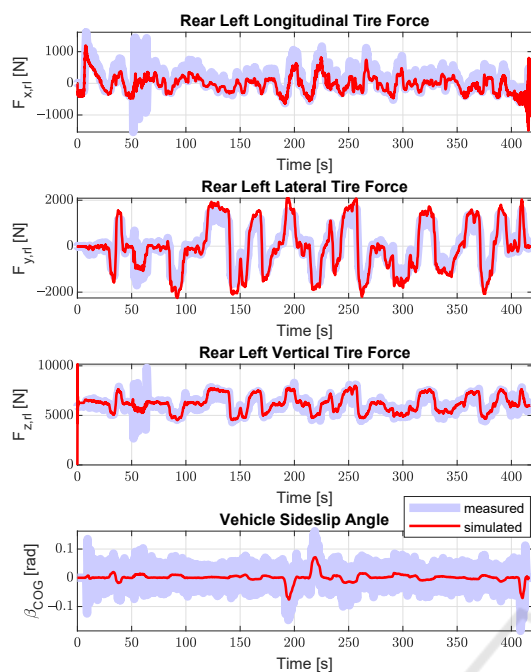


Figure 9: Estimation results for the rear left wheel forces and the vehicle sideslip angle.

objective estimators, one can observe that the sensors used for both tire force and sideslip angle estimation are mostly identical which is confirmed by the sensor selection results on figure 6. This approach is able to combine both quantities of interest in a single estimator and additionally provides improved performance due to the coupled dynamic nature of the model.

## 5 CONCLUSIONS

In this work, a novel, multi-objective, automotive state estimator has been developed featuring a system-level, non-linear vehicle model. As estimators using more complex models typically face more issues towards stability, an extensive observability analysis was performed. It is shown that unobservable states can be detected using a Singular Value Decomposition of the total observability matrix and that dynamic model coupling greatly determines the required sensors to obtain an observable estimator. Using an observable projection defined in previous work, this paper proves that it is possible to stabilize the estimator without GPS measurements if they are independent from the quantities of interest due to their decoupled nature. Finally, the estimator has been experimentally validated on an engineering vehicle case and proved to be able to accurately track all quantities of interest with a minimal sensor set.

## ACKNOWLEDGEMENTS

This research was partially supported by Flanders Make, the strategic research centre for the manufacturing industry. The Flanders Innovation & Entrepreneurship Agency within the IMPROVED and MULTISENSOR project is also gratefully acknowledged for its support. Internal Funds KU Leuven are gratefully acknowledged for their support.

## REFERENCES

- Albinsson, A., Bruzelius, F., Jonasson, M., and Jacobson, B. (2014). Tire force estimation utilizing wheel torque measurements and validation in simulations and experiments. In *12th International Symposium on Advanced Vehicle Control*, pages 294–299.
- Devos, T., Kirchner, M., Croes, J., Desmet, W., and Naets, F. (2021). Sensor selection and state estimation for unobservable and non-linear system models. *Sensors*, 21(22).
- Kim, D., Min, K., Kim, H., and Huh, K. (2020). Vehicle sideslip angle estimation using deep ensemble-based adaptive kalman filter. *Mechanical Systems and Signal Processing*, 144:106862.
- Naets, F., van Aalst, S., Boulkroune, B., Ghouti, N. E., and Desmet, W. (2017). Design and experimental validation of a stable two-stage estimator for automotive sideslip angle and tire parameters. *IEEE Transactions on Vehicular Technology*, 66(11):9727–9742.
- Nakamura, W., Hashimoto, T., and Chen, L.-K. (2020). State estimation method based on unscented kalman filter for vehicle nonlinear dynamics. *International Journal of Electrical and Information Engineering*, 14(12):435 – 438.
- Reif, K., Renner, K., and Saeger, M. (2007). Vehicle state estimation on the basis of a non-linear two-track model. *ATZ worldwide*, 109:33–36.
- Svendenius, J. and Wittenmark, B. (2003). Brush tire model with increased flexibility. In *European Control Conference*, pages 108–115.
- Van Aalst, S., Naets, F., Boulkroune, B., De Nijs, W., and Desmet, W. (2018). An adaptive vehicle sideslip estimator for reliable estimation in low and high excitation driving. In *15th IFAC Symposium on Control in Transportation Systems*, volume 51, pages 243–248.
- Vasseur, C., van Aalst, S., and Desmet, W. (2020). Vehicle state and tire force estimation: Performance analysis of pre and post sensor additions. In *2020 IEEE Intelligent Vehicles Symposium (IV)*, pages 1615–1620.
- Wang, R. and Wang, J. (2013). Tire–road friction coefficient and tire cornering stiffness estimation based on longitudinal tire force difference generation. *Control Engineering Practice*, 21(1):65–75.
- Yang, C., Blasch, E., and Douville, P. (2010). Design of schmidt-kalman filter for target tracking with navigation errors. In *IEEE Aerospace Conference Proceedings*, pages 1–12.